Allison R. Altman
McKay Orthopaedic Research Laboratory,
Department of Orthopaedic Surgery,
University of Pennsylvania,
424 Stemmler Hall,
36th Street and Hamilton Walk,
Philadelphia, PA 19104
e-mail: alaltman@mail.med.upenn.edu

Chantal M. J. de Bakker
McKay Orthopaedic Research Laboratory,
Department of Orthopaedic Surgery,
University of Pennsylvania,
424 Stemmler Hall,
36th Street and Hamilton Walk,
Philadelphia, PA 19104
e-mail: chantald@seas.upenn.edu

Wei-Ju Tseng
McKay Orthopaedic Research Laboratory,
Department of Orthopaedic Surgery,
University of Pennsylvania,
424 Stemmler Hall,
36th Street and Hamilton Walk,
Philadelphia, PA 19104
e-mail: weits@mail.med.upenn.edu

Abhishek Chandra
McKay Orthopaedic Research Laboratory,
Department of Orthopaedic Surgery,
University of Pennsylvania,
424 Stemmler Hall,
36th Street and Hamilton Walk,
Philadelphia, PA 19104
e-mail: abhic@mail.med.upenn.edu

Ling Qin
McKay Orthopaedic Research Laboratory,
Department of Orthopaedic Surgery,
University of Pennsylvania,
424A Stemmler Hall,
36th Street and Hamilton Walk,
Philadelphia, PA 19104
e-mail: qinling@mail.med.upenn.edu

X. Sherry Liu[1]
McKay Orthopaedic Research Laboratory,
Department of Orthopaedic Surgery,
University of Pennsylvania,
426C Stemmler Hall,
36th Street and Hamilton Walk,
Philadelphia, PA 19104
e-mail: xiaoweil@mail.med.upenn.edu

Enhanced Individual Trabecular Repair and Its Mechanical Implications in Parathyroid Hormone and Alendronate Treated Rat Tibial Bone

Combined parathyroid hormone (PTH) and bisphosphonate (alendronate—ALN) therapy has recently been shown to increase bone volume fraction and plate-like trabecular structure beyond either monotherapy. To identify the mechanism through which plate-like structure was enhanced, we used in vivo microcomputed tomography (μCT) of the proximal tibia metaphysis and individual trabecular dynamics (ITD) analysis to quantify connectivity repair (incidences of rod connection and plate perforation filling) and deterioration (incidences of rod disconnection and plate perforation). Three-month-old female, intact rats were scanned before and after a 12 day treatment period of vehicle (Veh, n = 5), ALN (n = 6), PTH (n = 6), and combined (PTH+ALN, n = 6) therapy. Additionally, we used computational simulation and finite element (FE) analysis to delineate the contributions of connectivity repair or trabecular thickening to trabecular bone stiffness. Our results showed that the combined therapy group had greater connectivity repair (5.8 ± 0.5% connected rods and 2.0 ± 0.3% filled plates) beyond that of the Veh group, resulting in the greatest net gain in connectivity. For all treatment groups, increases in bone volume due to thickening (5–31%) were far greater than those due to connectivity repair (2–3%). Newly formed bone contributing only to trabecular thickening caused a 10%, 41%, and 69% increase in stiffness in the ALN, PTH, and PTH+ALN groups, respectively. Moreover, newly formed bone that led to connectivity repair resulted in an additional improvement in stiffness, with the highest in PTH+ALN (by an additional 12%), which was significantly greater than either PTH (5.6%) or ALN (4.5%). An efficiency ratio was calculated as the mean percent increase in stiffness divided by mean percent increase in BV for either thickening or connectivity repair in each treatment. For all treatments, the efficiency ratio of connectivity repair (ALN: 2.9; PTH: 3.4; PTH+ALN: 4.4) was higher than that due to thickening (ALN: 2.0; PTH: 1.7; PTH+ALN: 2.2), suggesting connectivity repair required less new bone formation to induce larger gains in stiffness. We conclude that through rod connection and plate perforation filling PTH+ALN combination therapy improved bone stiffness in a more efficient and effective manner than either monotherapy. [DOI: 10.1115/1.4028823]

Keywords: In vivo μCT, three-dimensional (3D) image registration, trabecular connectivity, PTH treatment, antiresorptive treatment

Introduction

Aging shifts bone remodeling toward a negative balance between bone formation and resorption, causing bone loss and increased fracture risk. Antiresorptive agents such as bisphosphonates are commonly used to inhibit bone resorption and stabilize bone mass [1,2]. While anabolic treatment, such as intermittent parathyroid hormone (PTH), greatly stimulates bone formation [3–7]. Combined therapies of antiresorptive treatments and PTH have been proposed and are expected to further increase bone mass. Despite conflicting results in both clinical and preclinical studies [8–16], previous work in our lab has shown that combined therapy of PTH and alendronate (ALN), a bisphosphonate, results in an additive effect on bone volume fraction in intact

[1]Corresponding author.
Manuscript received June 16, 2014; final manuscript received September 30, 2014; accepted manuscript posted October 16, 2014; published online December 10, 2014. Assoc. Editor: Ara Nazarian.

 Copyright © 2015 by ASME

female rats [17]. While combined treatment and PTH monotreatment had a similar effect on stimulating new bone formation and improving trabecular thickness (Tb.Th), the addition of ALN to PTH further improves the relative bone volume and number of plate- versus rod-like structures [17].

Trabecular bone consists of a network of interconnected individual trabeculae, which can be classified as one of two major structural types, plate-like or rod-like trabeculae. While the majority of trabecular plates are axially aligned with the primary orientation of daily load-bearing, most trabecular rods horizontally connect trabecular plates to stabilize the overall structure [18–22]. Trabecular plates are often considered the most critical determinant of apparent bone strength as the plate-like trabecular bone volume is the strongest predictor of trabecular bone's elastic moduli and yield strength [18–23]. Despite minimal contributions to bone strength, trabecular rods play a significant role in failure initiation [18,20–22]. Furthermore, a mixture of plate and rod trabeculae ensures an open structure of trabecular bone to host bone marrow and blood vessels for the exchange of nutrients, waste, and calcium ions. Aging and metabolic bone diseases can lead to rapid bone loss that affects trabecular network integrity. Common structural changes in trabecular bone consist of thinning of trabeculae, trabecular plate perforation, and trabecular rod breakage. The latter two changes are more detrimental to bone strength: the perforation of trabecular plates causes a transition of plate-like to rod-like trabeculae while rod breakage leads to a reduced number of trabeculae. Using computational simulations of synthetic structure, it has been demonstrated that bone loss due to loss of trabecular elements has a greater impact on bone strength than due to trabecular thinning [24]. Moreover, without restoring the lost trabecular connectivity, bone strength cannot be fully restored by thickening of the remaining trabeculae [24]. This presents a major challenge for current osteoporosis treatments to not only prevent further bone loss but also to restore lost trabecular integrity by connectivity repair.

While the effect of the current available osteoporosis drug treatments on bone structure, mechanical properties, and fracture risk reduction have been extensively studied [1–17], there is limited data on their ability to enhance connectivity repair to restore lost mechanical function. This critical knowledge gap is partly due to the technical challenge of in vivo tracking of bone connectivity changes at an individual trabecula level. Most techniques currently available for microscale imaging of bone structure are limited to taking a "snapshot" of a complicated process. Recently, the development of in vivo μCT allows longitudinal imaging of trabecular bone microstructure at a resolution <15 μm, which enables the tracking of structural alterations at an individual trabecula level in rodent bone [25–31]. However, the challenges of precise registration of longitudinal scans as well as automatic detection of connectivity changes in individual trabecular structures remain. Our lab has developed an image analysis technique, individual trabecular dynamics (ITD) analysis, to track the changes within each individual trabecula over time. By ITD analysis, we can quantify the occurrences of individual trabecular connectivity deterioration, such as trabecular disconnection and perforation, and those of individual trabecular connectivity repair, such as trabecular connections and filled perforations. Thus, the first objective of the current study was to utilize the ITD analysis technique to monitor the temporal and spatial changes in individual trabeculae in the rat tibia in response to osteoporosis treatments. We aimed to elucidate detailed structural mechanisms through which PTH, bisphosphonate, and combined treatments can reverse bone connectivity deficits and increase plate-like trabeculae. The second objective was to determine how these changes in connectivity influence the mechanical function of the trabecular bone. Specifically, by computational simulation and finite element (FE) analysis, the mechanical contributions attributed to either trabecular thickening or connectivity repair were delineated for each treatment strategy.

In our recent studies, we have compared the changes in bone mass, microarchitecture, and mechanical stiffness due to 12 days of ALN, PTH, and combined treatment (PTH+ALN) in a rat model. Our results suggested the greatest treatment response in combined PTH+ALN therapy resulting in an additive effect of the two treatments due to greater plate-like trabecular structure. We hypothesized that the current study would reveal combined treatment to greatly enhance connectivity repair beyond that of either monotherapy. In addition, we hypothesized that this connectivity repair would occur due to PTH+ALN therapy in a highly efficient manner for improving trabecular bone stiffness.

Methods of Approach

Animals. A total of 30 female, 3-month-old, Sprague Dawley rats (Charles River Laboratories, Wilmington, MA) were assigned to vehicle (Veh, $n=6$), PTH ($n=9$), ALN ($n=6$), and combined PTH and ALN (PTH+ALN, $n=9$) treatment groups [17]. Beginning on day 0, the Veh and PTH groups received subcutaneous daily injections of either saline or human recombinant PTH 1–34 (PTH 1–34, 60 μg/kg/day, Bachem, Bubendorf, Switzerland), respectively, for 12 days. The ALN group received subcutaneous injections of 50 μg/kg ALN sodium trihydrate (Sigma Aldrich, St. Louis, MO) every 3 days with the first injection 3 days prior to day 0. The PTH+ALN group received both PTH and ALN treatments. A separate set of 4-month-old female rats ($n=10$) were used to assess the reproducibility of ITD analysis. All experiments were approved by the University of Pennsylvania's Institutional Animal Care and Use Committee.

In Vivo μCT Scans. In vivo μCT scans were performed for all groups at day 0, and the end of treatment (day 12) using a Scanco vivaCT 40 (Scanco Medical AG, Brüttisellen, Switzerland) at 10.5 μm nominal voxel size. The scanner energy was 55 keV energy, intensity = 142 μA, and integration time = 200 ms. Rats were anesthetized and immobilized during the scans (4.0/1.75% isoflurane) using a customized foot holder to ensure minimal motion over the 20 min scan [28]. A two-dimensional (2D) scout view was used to select the scan region, and a total of 417 slices (corresponding to a 4.4 mm region) distal to the proximal tibial growth plate were acquired. The same scan protocol was used to scan the tibia of the additional set of 10 female rats to assess the reproducibility of ITD analysis. These rats were scanned once, removed from the holder, repositioned, and scanned again. A total of 210 slices distal to the growth plate were acquired from each reproducibility scan.

Precise Image Registration of Trabecular Subvolumes. An open source software (National Library of Medicine Insight Segmentation and Registration Toolkit, USA) [32] was used to derive the transformation matrix between the image coordinates of baseline ($\mathbf{F}^1$) and follow-up ($\mathbf{F}^2$) μCT scans by landmark-initialized, mutual-information-based optimization [33,34]. This optimization scheme has been described in detail in a previous publication [28]. In the traditional registration scheme, once a transformation matrix $\mathbf{T}$ between image coordinates of baseline ($\mathbf{F}^1$) and follow-up ($\mathbf{F}^2$) scans is determined, it will be applied to move the follow-up scan into ($\mathbf{F}^1$). However, this approach would affect the image quality of the follow-up scan by image interpolation artifacts, making the baseline and transformed follow-up scans incomparable. Therefore, a new registration scheme was developed. Briefly, $\mathbf{T}$ was divided equally ($\mathbf{T}=\mathbf{T}_1\cdot\mathbf{T}_2^{-1}$; $\mathbf{T}_1=\mathbf{T}_2^{-1}$) so that one half of the rotation ($\mathbf{T}_1$) was applied to the follow-up image while the inverse of half of the rotation ($\mathbf{T}_2$) was applied to the baseline image. These transformations align the baseline and follow-up images in a new coordinate system ($\mathbf{F}^3$), resulting in minimized unequal resampling artifacts between scans (data not shown). The above registration scheme was applied to a $1.53\times1.53\times1.008$ mm^3 trabecular subvolume in the secondary spongiosa of the rat proximal tibia, corresponding to $146\times146\times96$ voxels. The subvolume was isolated in the baseline scan in the center of the trabecular compartment beginning approximately 2.5 mm distal to the proximal growth plate and

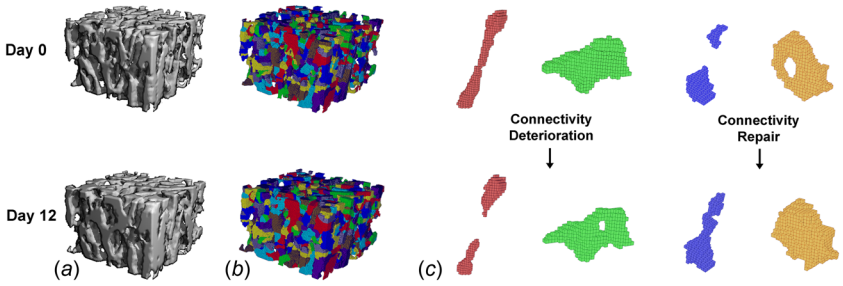

Fig. 1 (*a*) Precisely registered trabecular bone subvolumes from day 0 and day 12 treated by 12 days of PTH. (*b*) Individual rods and plates were isolated using ITS analysis, and occurrences of (*c*) rod disconnection, plate perforation, rod connection, and plate perforation filling (from left to right) were located and quantified by ITD analysis.

spanning to approximately 3.5 mm distal from the growth plate. The corresponding volume in the follow-up scan was then located by registration. Then, each registered grayscale image was thresholded using a Gaussian filter (sigma = 1.2, support = 2), and a global threshold corresponding to 545 mgHA/cm^3, determined based on previous data [17] (Fig. 1(*a*)). The registered, thresholded images of day 0 and day 12 were overlaid and each slice was manually examined to avoid misalignment due to local optima in the optimization algorithm. Standard trabecular microstructure analysis was performed within the registered trabecular subvolumes using Scanco software to evaluate standard bone microstructure parameters including bone volume fraction (BV/TV), trabecular thickness (Tb.Th), and connectivity density (Conn.D).

Individual Trabecular Dynamics (ITD) Analysis of Registered Trabecular Bone. Each pair of registered and thresholded baseline and day 12 scans was subjected to ITD analysis. First, using digital topological analysis (DTA) [35–37] and individual trabecula segmentation (ITS) analysis [19,23] the trabecular structure was decomposed and the individual trabecular plates and rods were isolated (Fig. 1(*b*)). Detailed methods describing the complete trabecular segmentation and volumetric decomposition technique can be found in our previous publications [19,23]. Once isolated, baseline and follow-up registered pairs were compared to identify incidences of connectivity repair and deterioration (Fig. 1(*c*)). Deteriorated connectivity was defined as plates or rods in the second scan which are perforated (plate perforation) or disconnected (rod disconnection) with respect to their initial topology. Repaired connectivity was defined as plates or rods in the second scan which are incomplete in the previous scan, incidences where holes in plates are filled (plate perforation filling), or disconnected rods are connected (rod connection). The percentages of rod disconnection, plate perforation, rod connection, and perforation filling were calculated as number of occurrences of the above connectivity changes normalized by the total number of trabeculae analyzed (468 trabeculae/sample on average) in each trabecular bone subvolume. The net connectivity gain was then defined as connectivity deterioration subtracted from connectivity repair (%plate perforation filling + %rod connection − %plate perforation − %rod disconnection). ITD analysis indicates the mechanisms of connectivity change on the individual trabecula level over the 12 day treatment period.

Precision of ITD Analysis. ITD analysis was also performed on the set of same-day repeated scans. Scans were registered and segmented as described above. The trabecular morphology should remain constant within the 40 min scan window, thus, connectivity repair and deterioration were expected to be 0. Any deviation from zero represents the precision error associated with the plate and rod measures. The percent incidence of rod connection and disconnection were averaged to represent the precision error for rods. Likewise, the percent incidence of plate perforation and plate perforation filling were averaged to determine the precision error for plates.

Micro Finite Element (μFE) Analyses of Registered Trabecular Bone. The precisely registered and thresholded subvolumes from baseline and follow-up of all treatment groups (ALN, PTH, and PTH+ALN) were constructed into μFE models for trabecular bone stiffness measurement [38] by converting each bone voxel to an eight-node brick element. Bone tissue was modeled as an isotropic, linear elastic material with a Young's modulus (E_s) of 15 GPa and a Poisson's ratio of 0.3 [39]. A uniaxial compression test was performed to calculate the reaction force under a 0.01 mm displacement along the axial direction of the bone. A linear elastic analysis was performed on the μFE model using an element-by-element preconditioned conjugate gradient solver [40]. Then, the trabecular bone stiffness was derived as the reaction force divided by the applied displacement.

Computational Simulation to Evaluate the Contribution of Trabecular Thickening and Connectivity Repair to Bone Volume and Stiffness by Different Treatments. Based on the day 0 and day 12 images, an additional 3D image volume was generated for ALN, PTH, and ALN+PTH groups, so that the effects of altered connectivity were removed by replacing locations of altered connectivity at day 12, determined by ITD, with pretreatment connectivity at day 0 (illustrated in a 2D image in Fig. 2). Therefore, in the simulated image, the treatment effect due to trabecular thickening was present while all the connectivity identified by ITD was removed. In contrast, in the day 12 image, the treatment effect due to both thickening and connectivity change was present. Subsequently, stiffness was determined for

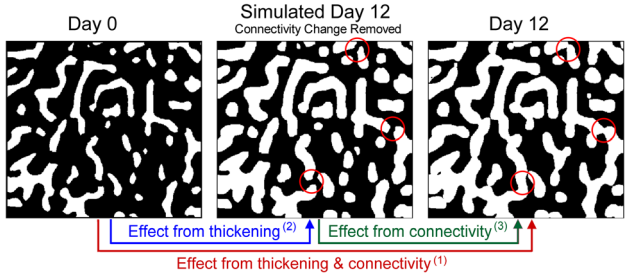

Fig. 2 2D schematics for the 3D μFE analysis performed on the day 0 (left), day 12 (right), and simulated day 12 image (middle). The simulated image was created by deleting the effects of changed connectivity over the treatment period identified by ITD analysis. Circles indicate examples of locations where altered connectivity was returned to baseline. The arrows below describe how each structural contribution was delineated, numbers correspond to Eqs. (1)–(3).

day 0 (Stiff.d0) and day 12 (Stiff.d12) images as well as for the simulated model (Stiff′) of each treatment group (Fig. 2). The difference between Stiff′ and Stiff.d0 reflects the mechanical improvement due to trabecular thickening only, while the difference between Stiff.d12 and Stiff′ reflects the mechanical improvement due to connectivity gain only. Similarly, the bone volume (BV) that was associated with each image (day 0, day 12, and the simulated image) was also calculated (BV.d0, BV.d12, and BV′). Further calculations were done to determine the independent contribution of thickening and connectivity repair to bone stiffness increase based on the following equations (Fig. 2):

$$\frac{\text{Stiff}.d12 - \text{Stiff}.d0}{\text{Stiff}.d0} = \% \text{ Increase in stiffness due to thickening and connectivity repair} \quad (1)$$

$$\frac{\text{Stiff}' - \text{Stiff}.d0}{\text{Stiff}.d0} = \% \text{ Increase in stiffness due to thickening only} \quad (2)$$

$$\frac{\text{Stiff}.d12 - \text{Stiff}'}{\text{Stiff}.d0} = \% \text{ Increase in stiffness due to connectivity repair only} \quad (3)$$

Similarly, the contributions of thickening and connectivity repair to BV increase were also evaluated. To describe how efficiently new bone was formed to improve stiffness for each treatment, an efficiency ratio was calculated for each group by dividing the mean percent increase in stiffness by the mean percent increase in BV. Efficiency ratio was calculated separately for each treatment type due to either thickening or connectivity repair.

Statistical Analysis. All statistical analyses were performed using NCSS 7.1.14 (NCSS, LLC, Kaysville, UT). Results were presented as mean ± standard error. All the assumptions for parametric tests were evaluated and confirmed for each variable. For ITD measurements a one-way analysis of variance (ANOVA) was used to compare treatment groups. In the presence of statistically significant ANOVA, post hoc comparisons of between-group differences were made using a Bonferroni correction. Net connectivity gain was calculated by subtracting connectivity deterioration from connectivity repair. Correlation analysis was performed to compare net connectivity gain to Conn.D calculated by standard microstructural analysis. Pearson's correlations were also performed to determine the contributions of BV/TV, Tb.Th, and ITD net connectivity gain to stiffness. Changes in BV and stiffness due to thickening and connectivity repair were evaluated by a two-way mixed model ANOVA, where time was considered a repeated measure, and changes over time were compared across treatment groups. Baseline values were used as a covariate to normalize between rats. In the presence of a significant interaction effect, post hoc comparisons were made between groups and over time using a Bonferroni correction to assess differences in the percent increases in BV and stiffness. For all analyses, a two-tailed $p \leq 0.05$ was considered to indicate statistical significance, and $p \leq 0.1$ was considered a trend toward significance. Unless otherwise noted, all differences discussed reached statistical significance ($p \leq 0.05$).

Results

Standard Trabecular Bone Microstructure Analysis. The accuracy of ITD analysis was highly reliant on scan quality. Images from 7 out of the 30 rats were excluded due to insufficient image quality caused by motion artifact at either day 0 and/or day 12. Therefore, all subsequent analysis was performed only in the remaining images (Veh: $n = 5$, ALN: $n = 6$, PTH: $n = 6$, PTH+ALN: $n = 6$).

Similar to what has been reported in a previous study [17], BV/TV was increased over the treatment period for all treatment groups (7% ALN, 26% PTH, and 34% PTH+ALN), but unchanged in the Veh group with a BV/TV equal to 0.23 (Fig. 3(*a*)). By the end of treatment, BV/TV in each treatment group was greater than that of the Veh group by 11% (ALN), 32% (PTH), and 53% (PTH+ALN). The combined treatment group was significantly higher than both ALN and PTH monotreatment groups by 38% and 16%, respectively. The differences between groups were further magnified when looking at changes in stiffness (Fig. 3(*b*)). Over 12 days of treatment, trabecular bone stiffness was increased by 15% in ALN, 47% in PTH, and 80% in the PTH+ALN groups. At day 12, the stiffness of the three treatment groups was 29–100% greater than that of the Veh group. The PTH+ALN group had the highest stiffness compared to either ALN (55%) or PTH (20%). At day 12, Tb.Th in PTH and PTH+ALN groups was 22–23% greater than that of the Veh group (Fig. 3(*c*)). Due to high variance in the Conn.D measure, there was no change detected in Conn.D over time or between groups at day 12 (Fig. 3(*d*)).

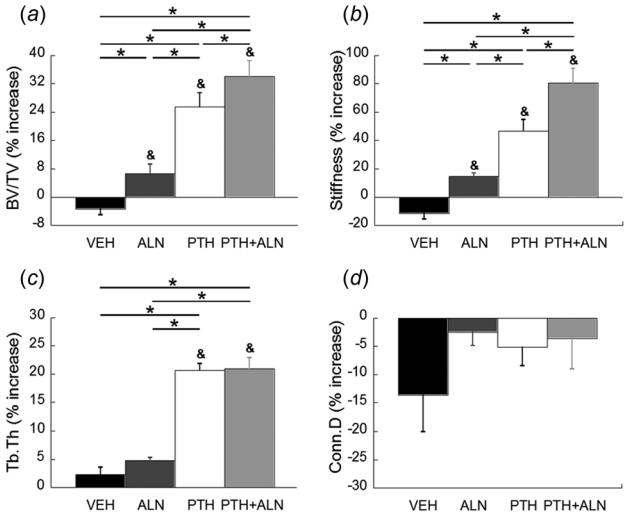

Fig. 3 Standard trabecular microstructural evaluation on precisely registered subvolumes: (*a*) BV/TV, (*b*) stiffness, (*c*) Tb.Th, and (*d*) Conn.D. Bar graphs represent the percent difference from baseline to day 12 of each parameter. "*" Indicates a significant difference between groups at day 12, and "&" indicates a significant increase from baseline.

Precision of ITD Analysis. The same-day repeated tibial scans revealed a low incidence of rod and plate repair and deterioration. Specifically, the precision error was found to be 0.81% for detecting connectivity changes in trabecular rods, and 0.27% for trabecular plates. This was considered an acceptable margin for error.

ITD Analyses of Registered In Vivo Trabecular Bone Images. The tracking of individual trabecular connectivity over the course of treatment indicated several rod disconnections and plate perforations even in the Veh-treated bone (3.2 ± 1.0% and 0.6 ± 0.2% of the total trabeculae, respectively, Fig. 4). This was balanced by similar connectivity repair with 2.0 ± 0.7% connected rods and 0.7 ± 0.2% filled plates. In the ALN-treated group this balance was tipped toward connectivity repair with 3.7 ± 1.1% connected rods, and 1.0 ± 0.3% filled plates. Interestingly, the PTH-treated group had a similar amount of connectivity repair (3.9 ± 0.7% connected rods and 1.3 ± 0.2% filled plates) to that of the ALN group. In addition, the PTH group tended to have a lower incidence of plate perforation (0.1 ± 0.1%, $p < 0.1$) compared with the Veh group. The combined PTH+ALN-treated group tended to have reduced rod disconnection (0.7 ± 0.5%, $p < 0.1$) and plate perforation (0.1 ± 0.1%, $p < 0.1$), and displayed greater connectivity repair (5.8 ± 0.5% connected rods, and

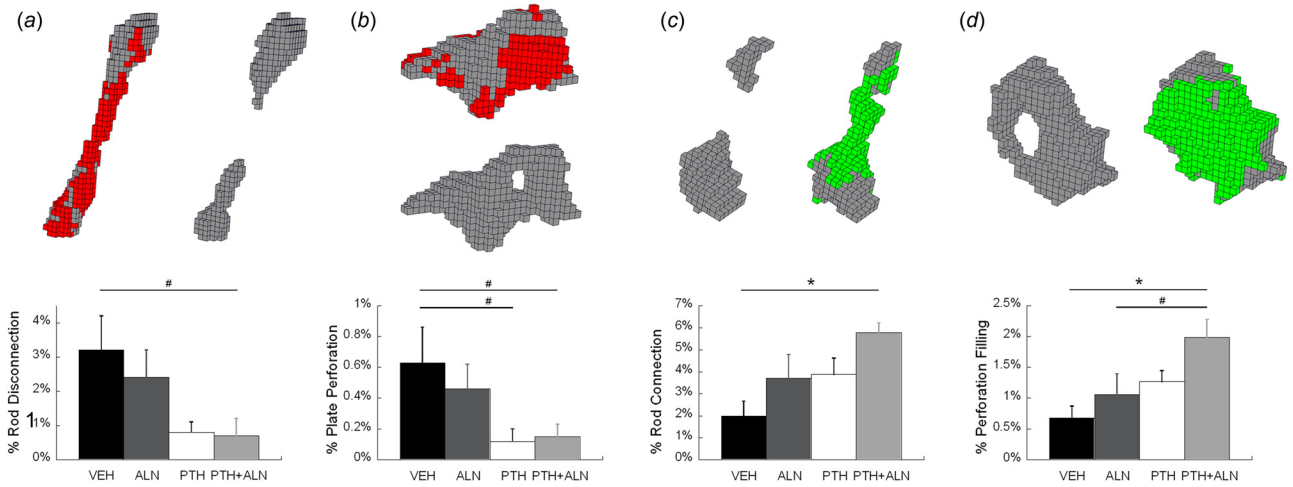

Fig. 4 (Top) Representative images of ITD: (*a*) rod disconnection; (*b*) plate perforation; (*c*) rod connection; and (*d*) perforation filling. Each brick represents an image voxel ($10.5 \times 10.5 \times 10.5\ \mu m^3$). Red/darker shading indicates the bone tissue lost at day 12 in (*a*) and (*b*) and green/lighter shading indicates the bone tissue gained at day 12 in (*c*) and (*d*). (Bottom) percent of (*a*) rod disconnection, (*b*) plate perforation, (*c*) rod connection, and (*d*) perforation filling over total number of trabeculae were compared among Veh, ALN, PTH, and PTH+ALN groups. "*" Significant difference between treatment groups; "#" trend difference ($p < 0.1$) between treatment groups.

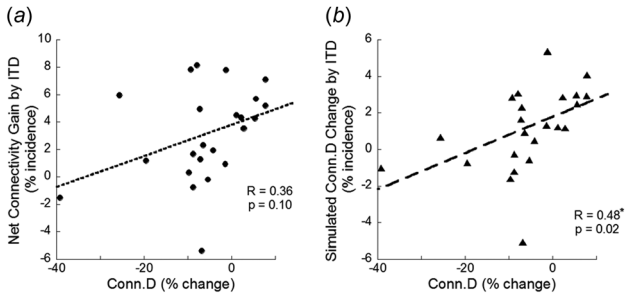

Fig. 5 Linear correlation between standard Conn.D measurement and (*a*) ITD measures of net connectivity gain (connectivity deterioration subtracted from connectivity repair) and (*b*) ITD measures of simulated Conn.D (%plate perforation − %plate perforation filling + %rod connection − %rod disconnection). "*" Indicates a significant correlation.

$2.0 \pm 0.3\%$ filled plates, $p < 0.05$) beyond that of the Veh group, resulting in the greatest net gain in connectivity. All treatment differences found were beyond the precision error of ITD measurements for both rods and plates.

Comparison of ITD to Conn.D Measurement. Net connectivity gain, calculated by subtracting ITD measures of deteriorated connectivity from those of repaired connectivity (%plate perforation filling − %plate perforation + %rod connection − %rod disconnection), was not correlated with Conn.D (Fig. 5(*a*)). By the definition of Conn.D, plate perforation and rod connection contribute to an increase in Conn.D and plate perforation filling and rod disconnection contribute to decreased Conn.D [41–44]. Therefore, we calculated an equivalent ITD parameter (%plate perforation − %perforation filling + %rod connection − %rod disconnection) to be comparable with the traditional Conn.D measurement. This modified ITD connectivity calculation was significantly correlated with Conn.D with a correlation coefficient of 0.48 (Fig. 5(*b*)).

Correlations Between Trabecular Bone Structural Improvements and Increased Stiffness. The percent increase in stiffness was highly correlated with the increase in BV/TV with a correlation coefficient of 0.98 (Fig. 6(*a*)). This increase in BV/TV is attributed to improvements due to thickening (Tb.Th) and net connectivity gain (connectivity repair subtracted by connectivity deterioration). Not surprisingly, the increased Tb.Th was highly correlated to increased stiffness with a correlation coefficient of 0.88 (Fig 6(*b*)). Despite alterations in a small number of trabecular structures (7% on average/sample), net connectivity gain by ITD also was significantly correlated with increased stiffness with a correlation coefficient of 0.84 (Fig. 6*c*).

Contributions of Trabecular Thickening and Connectivity Repair to Bone Volume and Stiffness by Different Treatments. For all treatment groups, the increases in BV due to thickening

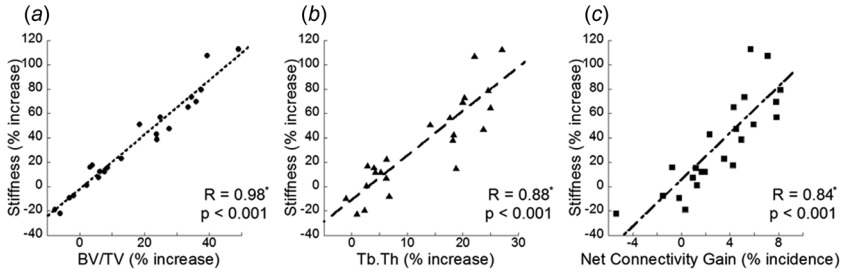

Fig. 6 Linear correlation of percent increase in stiffness and percent increase in (*a*) BV/TV, (*b*) Tb.Th, and (*c*) ITD measures of net connectivity gain (connectivity deterioration subtracted from connectivity repair). "*" Indicates a significant correlation.

Table 1 Percent increase in BV and stiffness due to thickening and connectivity repair

	ALN	PTH	PTH+ALN
BV (%increase)			
Due to thickening	$5.1 \pm 1.4^{b,c}$	23.9 ± 3.7^{a}	31.3 ± 4.6^{a}
Due to connectivity repair	1.5 ± 0.6	1.7 ± 0.4	2.7 ± 0.2
Stiffness (%increase)			
Due to thickening	$10.3 \pm 2.0^{b,c}$	$41.0 \pm 6.8^{a,c}$	$68.5 \pm 10.1^{a,b}$
Due to connectivity repair	4.5 ± 1.9^{c}	5.6 ± 1.4^{c}	$11.9 \pm 0.9^{a,b}$

Note: Superscript letters indicate significant differences from [a]ALN, [b]PTH, and [c]PTH+ALN groups.

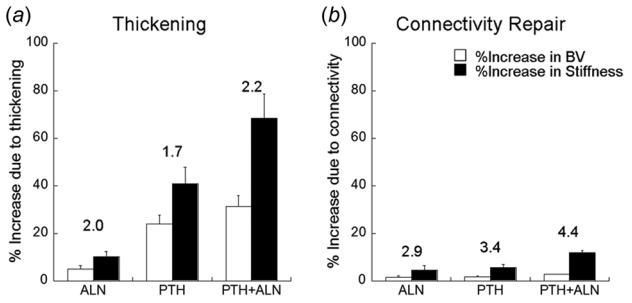

Fig. 7 Percent increase in BV and stiffness attributed to (*a*) thickening and (*b*) connectivity repair in each treatment group. Numbers over bars indicate the efficiency ratio for a particular treatment and mechanism.

(5–31%) were far greater than those due to connectivity repair (2–3%, Table 1, Fig. 7). Thickening was the primary contributor to increased stiffness, accounting for 10–68% increases in stiffness for each treatment group. Despite a small contribution to BV, connectivity repair led to an additional 5–12% improvement in stiffness.

Both thickening and connectivity repair contributed to the additive effect on BV and stiffness in the combined therapy group over either monotherapy. BV increases due to thickening were higher in PTH (24%) and PTH+ALN (31%) than ALN (5%), while BV increases due to connectivity repair were minimal and not different between all three treatments (2–3%). Stiffness increase due to both thickening and connectivity repair was highest in PTH+ALN (69% and 12%, respectively). Stiffness increase due to thickening was higher in PTH than ALN (41% and 10%, respectively), while stiffness increase due to connectivity was not different between the two treatments (5% and 6%, respectively). The efficiency ratio was calculated as the mean percent increase in stiffness divided by mean percent increase in BV, caused by either thickening or connectivity repair. For thickening, the efficiency ratio was between 1.7 and 2.2 for all treatment groups. For all treatments, the efficiency ratio of connectivity repair was higher than that due to thickening. There was a moderate efficiency ratio for connectivity repair in both monotreatments of 2.9 (ALN) and 3.4 (PTH). The highest efficiency was observed in the PTH+ALN group due to connectivity repair with a ratio of 4.4.

Discussion

The current study suggests that combined therapy of PTH and ALN not only has an additive effect on bone volume but also on trabecular stiffness through increased trabecular thickness and improved connectivity. This novel ITD method was able to isolate individual incidences of plate and rod repair over a treatment period to quantify structural connectivity repair on the individual trabecular level. The present work showed that combined PTH and ALN therapy induces a more targeted structural repair than either PTH or ALN monotherapy. Furthermore, ITD allowed for the automatic detection of the effects of changed connectivity to delineate its effects on mechanical function. This powerful application revealed the highly efficient nature of combined therapy for specifically targeting connectivity repair and improving mechanical stiffness.

The results from this study further elucidate the additive effects in bone volume fraction observed in our previous study [17]. Previous reports show that ALN primarily prevents resorption, resulting in stable bone structure [1,2], and that PTH primarily induces new bone formation, resulting in increased trabecular thickness [3–7]. While these young, healthy ALN-treated rats did not display any reduction in connectivity deterioration compared to Veh, the addition of ALN to PTH resulted in a significant reduction in connectivity deterioration of both rod and plate trabeculae. The additive effect of combined PTH and anticatabolic therapy is supported by a growing body of existing literature [10,15,16,45–49]. Our previous work showed that increased trabecular thickening was similar in both PTH and PTH+ALN groups, and suggested the additive effect may be related to the higher occurrence of plate-like trabeculae [17]. However, the traditional method of examining connectivity by Conn.D detected no changes in any treatment group over time. In the current study, ITD analysis allows us to observe individual connectivity events over time to make distinctions between various connectivity deterioration and repair mechanisms. As such, combined therapy was found to offer a maximal protective effect by both reduced deterioration (fewer rods disconnected and plates perforated) and increased connectivity repair (more rod connections and filled plate perforations), consistent with our hypothesis.

Though it did not reach statistical significance, occurrences of rod connection and perforation filling were in general higher in the ALN versus Veh group, and also higher in the PTH+ALN versus PTH group. Our previous data also showed that ALN with or without concurrent treatment of PTH promotes plate-like trabecular structure, suggesting ALN may have an osteogenic function in addition to its antiresorptive effect. This is consistent with previous in vitro reports that bisphosphonates, especially ALN, promote osteoblastogenesis of mesenchymal progenitors and osteoblastic cells [50–52]. Since the overall frequencies of connected rods and filled perforations are low (2–5% and 0.5–2%, respectively), these increases are not sufficient to alter the measured trabecular thickness and bone formation rate calculation. However, this effect might be critical for the alendronate-induced, targeted bone formation to increase bone strength.

While the mechanism of targeted osteoblastogenesis is unknown, deteriorated structure may induce increased stress to initiate bone remodeling. We speculate that small gaps between disconnected rods and inside perforations may increase the fluid shear stress along the surface of bone tissue, while perforated plates may induce stress concentration in the bone tissue. The response to these mechanical stimuli may be amplified by either ALN or PTH administration. In addition, a growing pool of literature suggests that PTH's action is partially regulated by local mechanical signaling, which may play a role in recruiting progenitors and osteoblasts to sites of high stress in either the tissue or marrow [53–55].

In this study, we used bone stiffness as the most important outcome to evaluate osteoporosis treatment efficacy. By linear correlation analysis, we demonstrated that percent increase in bone volume was the strongest predictor of the percent increase in bone stiffness ($R = 0.98$), the primary treatment efficacy outcome. Furthermore, percent increase in trabecular thickness and ITD-based connectivity gain, were also strong predictors of percent increase in bone stiffness ($R = 0.88$ and 0.84, respectively). The mechanical contributions of both thickening and connectivity repair were also delineated using computational simulation and μFE analysis. Thickening was the dominant contributor to stiffness in all groups, with the highest, additive contribution in the PTH+ALN group. Connectivity repair contributed to stiffness to a much lesser degree in all treatments. However, connectivity repair required

less new bone formation to induce larger gains in stiffness. Compared to the efficiency of thickening, connectivity repair was almost twice as efficient for promoting increased trabecular bone stiffness, again with the greatest contribution and efficiency ratio in the PTH+ALN group. Our results are consistent with a previous study by Guo and Kim, which used a computer simulation of synthetic structure to demonstrate that repairing lost trabecular connectivity is the most effective means to recover mechanical properties while trabecular thickening only partially restores mechanical properties [24]. Combined with the current data, this suggests that connecting trabecular rods and filling trabecular plate perforations are critical mechanisms through which combination therapy can more efficiently restore mechanical function to osteoporotic bone.

While the present study showed novel experimental findings which elucidate the additive effects of combined therapy, it had limiting factors. First, the sample size of the current study was small. The addition of more samples is expected to further increase the differences observed, thus strengthening the current findings. The precise alignment of baseline and follow-up scans is highly sensitive to scan quality, and accurate evaluation of connectivity through ITD relies heavily on exact alignment of the two scans. Thus, in vivo μCT scans with large motion artifact or reduced signal-to-noise ratio cannot be included for the ITD analysis. Furthermore, the rotation and thresholding of these scans subjects them to a further reduction in image quality through resampling and partial volume effects. In the present work, steps were taken to optimize scan quality by fixing the rat tibia in place, and closely monitoring the animals while under anesthesia. The effects of resampling and partial volume were minimized using the registration method described, and a global threshold determined by a thorough adaptive method [17]. In addition, treatment differences were well above the precision error for both rod and plate connectivity detection. While the simple axial μFE analysis was able to deduce meaningful information to delineate the mechanical contributions of structural improvements, it oversimplifies the loading in vivo. It is possible that connectivity repair has an even greater contribution to mechanical function in torsion, or more complex loading conditions. In addition, this μFE model did not incorporate differences in bone tissue properties due to treatment. Both PTH and ALN treatments may have an effect on the bone tissue properties; however, based on previous data we expect the magnitude of these changes to be small [17], and by definition, linearly related to stiffness, and would not alter the current findings. An alternative approach to evaluate the contribution of connectivity repair and trabecular thickening was to generate a simulated $d12$ image with changes in thickness removed but those in connectivity remaining. This was not tested in the current study. However, we would expect similar conclusions with the alternative simulation approach and both methods will be verified in our future study. Finally, the differences observed between treatments were in a young, intact rat model. However, even in this intact model with a limited capacity for improvement, we observed substantial gains in trabecular connectivity. A similar study is currently ongoing to test these results in an older ovariectomized rat model.

Despite the limitations, this paper also has unique strengths. The current standard method for evaluating trabecular connectivity is through measurement of Conn.D [41–44]. This method is highly sensitive to the amount of bone present, and often over or under-represents the actual connectivity. In the present work, Conn.D was not correlated with ITD measures of net connectivity gain. This is likely due to a shortcoming in Conn.D determination, which makes no distinction between rod and plate connections, and would classify a plate perforation as an increase in Conn.D. Since plate-structure plays a key role in the mechanical competence of trabecular bone, this occurrence should not be quantified as a beneficial change in connectivity. The ITD analysis not only improves upon the detection of connectivity in a manner correlated with mechanical competence, but it also describes changes in connectivity over time. This technique afforded us the ability to precisely quantify connectivity repair and deterioration between different treatment types. Unlike Conn.D, ITD analysis revealed important differences between treatment groups that had a substantial impact on the resulting mechanical function. This will be an important tool for comparing the function of future drug therapies, as well.

Conclusion

Overall, this study demonstrates the structural mechanism through which combined PTH and ALN therapy improves trabecular bone mechanical function. The novel techniques used in this study demonstrate the importance of connectivity repair for improving trabecular bone stiffness. Connectivity repair is a highly efficient way to improve bone stiffness with minimal, but targeted, new bone formation. Combined therapy appears to cause greater connectivity repair, thus most efficiently improving bone stiffness. Since lost trabecular connectivity is far more detrimental to bone strength than uniform thinning of trabeculae [24], it is crucial to understand the degree to which connectivity can be repaired and mechanical competence restored by current osteoporosis treatments. This method shows great potential to become a promising tool in evaluating osteoporosis treatment efficacy by its ability to improve trabecular connectivity, thus increase bone mechanical function.

Acknowledgment

This study was partially supported by McCabe Pilot Award (to X.S.L.), Penn Center for Musculoskeletal Disorders (PCMD) and National Institute of Health (NIH) (NIH/NIAMS P30-AR050950), American Society of Bone and Mineral Research (ASBMR) Junior Faculty Osteoporosis Basic Research Award (to L.Q.), NIH/NIDDK R01-DK09580301 (to L.Q.), and NIH/NIAMS T32-AR007132 (to C.M.J.dB).

References

[1] Bone, H. G., Hosking, D., Devogelaer, J. P., Tucci, J. R., Emkey, R. D., Tonino, R. P., Rodriguez-Portales, J. A., Downs, R. W., Gupta, J., Santora, A. C., and Liberman, U. A., 2004, "Ten Years' Experience With Alendronate for Osteoporosis in Postmenopausal Women," N. Engl. J. Med., **350**(12), pp. 1189–1199.

[2] McClung, M., Harris, S. T., Miller, P. D., Bauer, D. C., Davison, K. S., Dian, L., Hanley, D. A., Kendler, D. L., Yuen, C. K., and Lewiecki, E. M., 2013, "Bisphosphonate Therapy for Osteoporosis: Benefits, Risks, and Drug Holiday," Am. J. Med., **126**(1), pp. 13–20.

[3] Baron, R., and Hesse, E., 2012, "Update on Bone Anabolics in Osteoporosis Treatment: Rationale, Current Status, and Perspectives," J. Clin. Endocrinol. Metab., **97**(2), pp. 311–325.

[4] Datta, N. S., and Abou-Samra, A. B., 2009, "PTH and PTHrP Signaling in Osteoblasts," Cell. Signalling, **21**(8), pp. 1245–1254.

[5] Goltzman, D., 2008, "Studies on the Mechanisms of the Skeletal Anabolic Action of Endogenous and Exogenous Parathyroid Hormone," Arch. Biochem. Biophys., **473**(2), pp. 218–224.

[6] Jilka, R. L., 2007, "Molecular and Cellular Mechanisms of the Anabolic Effect of Intermittent PTH," Bone, **40**(6), pp. 1434–1446.

[7] Qin, L., Raggatt, L. J., and Partridge, N. C., 2004, "Parathyroid Hormone: A Double-Edged Sword for Bone Metabolism," Trends Endocrinol. Metab., **15**(2), pp. 60–65.

[8] Black, D. M., Greenspan, S. L., Ensrud, K. E., Palermo, L., McGowan, J. A., Lang, T. F., Garnero, P., Bouxsein, M. L., Bilezikian, J. P., and Rosen, C. J., 2003, "The Effects of Parathyroid Hormone and Alendronate Alone or in Combination in Postmenopausal Osteoporosis," N. Engl. J. Med., **349**(13), pp. 1207–1215.

[9] Cosman, F., Eriksen, E. F., Recknor, C., Miller, P. D., Guanabens, N., Kasperk, C., Papanastasiou, P., Readie, A., Rao, H., Gasser, J. A., Bucci-Rechtweg, C., and Boonen, S., 2011, "Effects of Intravenous Zoledronic Acid Plus Subcutaneous Teriparatide [rhPTH(1–34)] in Postmenopausal Osteoporosis," J. Bone Miner. Res., **26**(3), pp. 503–511.

[10] Cosman, F., Keaveny, T. M., Kopperdahl, D., Wermers, R. A., Wan, X., Krohn, K. D., and Krege, J. H., 2013, "Hip and Spine Strength Effects of Adding Versus Switching to Teriparatide in Postmenopausal Women With Osteoporosis Treated With Prior Alendronate or Raloxifene," J. Bone Miner. Res., **28**(6), pp. 1328–1336.

[11] Cosman, F., Nieves, J., Zion, M., Woelfert, L., Luckey, M., and Lindsay, R., 2005, "Daily and Cyclic Parathyroid Hormone in Women Receiving Alendronate," N. Engl. J. Med., **353**(6), pp. 566–575.

[12] Cosman, F., Wermers, R. A., Recknor, C., Mauck, K. F., Xie, L., Glass, E. V., and Krege, J. H., 2009, "Effects of Teriparatide in Postmenopausal Women With Osteoporosis on Prior Alendronate or Raloxifene: Differences Between Stopping and Continuing the Antiresorptive Agent," J. Clin. Endocrinol. Metab., **94**(10), pp. 3772–3780.
[13] Finkelstein, J. S., Hayes, A., Hunzelman, J. L., Wyland, J. J., Lee, H., and Neer, R. M., 2003, "The Effects of Parathyroid Hormone, Alendronate, or Both in Men With Osteoporosis," N. Engl. J. Med., **349**(13), pp. 1216–1226.
[14] Finkelstein, J. S., Wyland, J. J., Lee, H., and Neer, R. M., 2010, "Effects of Teriparatide, Alendronate, or Both in Women With Postmenopausal Osteoporosis," J. Clin. Endocrinol. Metab., **95**(4), pp. 1838–1845.
[15] Muschitz, C., Kocijan, R., Fahrleitner-Pammer, A., Lung, S., and Resch, H., 2013, "Antiresorptives Overlapping Ongoing Teriparatide Treatment Result in Additional Increases in Bone Mineral Density," J. Bone Miner. Res., **28**(1), pp. 196–205.
[16] Schafer, A. L., Burghardt, A. J., Sellmeyer, D. E., Palermo, L., Shoback, D. M., Majumdar, S., and Black, D. M., 2013, "Postmenopausal Women Treated With Combination Parathyroid Hormone (1–84) and Ibandronate Demonstrate Different Microstructural Changes at the Radius vs. Tibia: The PTH and Ibandronate Combination Study (PICS)," Osteoporos. Int., **24**(10), pp. 2591–2601.
[17] Altman, A. R., Tseng, W. J., de Bakker, C. M., Huh, B. K., Chandra, A., Qin, L., and Liu, X. S., 2014, "A Closer Look at the Immediate Trabecula Response to Combined Parathyroid Hormone and Alendronate Treatment," Bone, **61C**, pp. 149–157.
[18] Liu, X. S., Bevill, G., Keaveny, T. M., Sajda, P., and Guo, X. E., 2009, "Micromechanical Analyses of Vertebral Trabecular Bone Based on Individual Trabeculae Segmentation of Plates and Rods," J. Biomech., **42**(3), pp. 249–256.
[19] Liu, X. S., Sajda, P., Saha, P. K., Wehrli, F. W., Bevill, G., Keaveny, T. M., and Guo, X. E., 2008, "Complete Volumetric Decomposition of Individual Trabecular Plates and Rods and Its Morphological Correlations With Anisotropic Elastic Moduli in Human Trabecular Bone," J. Bone Miner. Res., **23**(2), pp. 223–235.
[20] Liu, X. S., Zhang, X. H., and Guo, X. E., 2009, "Contributions of Trabecular Rods of Various Orientations in Determining the Elastic Properties of Human Vertebral Trabecular Bone," Bone, **45**(2), pp. 158–163.
[21] Shi, X., Liu, X. S., Wang, X., Guo, X. E., and Niebur, G. L., 2010, "Type and Orientation of Yielded Trabeculae During Overloading of Trabecular Bone Along Orthogonal Directions," J. Biomech., **43**(13), pp. 2460–2466.
[22] Shi, X., Liu, X. S., Wang, X., Guo, X. E., and Niebur, G. L., 2010, "Effects of Trabecular Type and Orientation on Microdamage Susceptibility in Trabecular Bone," Bone, **46**(5), pp. 1260–1266.
[23] Liu, X. S., Sajda, P., Saha, P. K., Wehrli, F. W., and Guo, X. E., 2006, "Quantification of the Roles of Trabecular Microarchitecture and Trabecular Type in Determining the Elastic Modulus of Human Trabecular Bone," J. Bone Miner. Res., **21**(10), pp. 1608–1617.
[24] Guo, X. E., and Kim, C. H., 2002, "Mechanical Consequence of Trabecular Bone Loss and Its Treatment: A Three-Dimensional Model Simulation," Bone, **30**(2), pp. 404–411.
[25] Boyd, S. K., Davison, P., Muller, R., and Gasser, J. A., 2006, "Monitoring Individual Morphological Changes Over Time in Ovariectomized Rats by In Vivo Micro-Computed Tomography," Bone, **39**(4), pp. 854–862.
[26] Brouwers, J. E., van Rietbergen, B., and Huiskes, R., 2007, "No Effects of In Vivo Micro-CT Radiation on Structural Parameters and Bone Marrow Cells in Proximal Tibia of Wistar Rats Detected After Eight Weekly Scans," J. Orthop. Res., **25**(10), pp. 1325–1332.
[27] Buie, H. R., Moore, C. P., and Boyd, S. K., 2008, "Postpubertal Architectural Developmental Patterns Differ Between the L3 Vertebra and Proximal Tibia in Three Inbred Strains of Mice," J. Bone Miner. Res., **23**(12), pp. 2048–2059.
[28] Lan, S., Luo, S., Huh, B. K., Chandra, A., Altman, A. R., Qin, L., and Liu, X. S., 2013, "3D Image Registration is Critical to Ensure Accurate Detection of Longitudinal Changes in Trabecular Bone Density, Microstructure, and Stiffness Measurements in Rat Tibiae by in vivo Micro Computed Tomography (μCT)," Bone, **56**(1), pp. 83–90.
[29] Schulte, F. A., Lambers, F. M., Kuhn, G., and Muller, R., 2011, "In Vivo Micro-Computed Tomography Allows Direct Three-Dimensional Quantification of Both Bone Formation and Bone Resorption Parameters Using Time-Lapsed Imaging," Bone, **48**(3), pp. 433–442.
[30] Waarsing, J. H., Day, J. S., van der Linden, J. C., Ederveen, A. G., Spanjers, C., De Clerck, N., Sasov, A., Verhaar, J. A., and Weinans, H., 2004, "Detecting and Tracking Local Changes in the Tibiae of Individual Rats: A Novel Method to Analyse Longitudinal In Vivo Micro-CT Data," Bone, **34**(1), pp. 163–169.
[31] Chandra, A., Lan, S., Zhu, J., Lin, T., Zhang, X., Siclari, V. A., Altman, A. R., Cengel, K. A., Liu, X. S., and Qin, L., 2013, "PTH Prevents the Adverse Effects of Focal Radiation on Bone Architecture in Young Rats," Bone, **55**(2), pp. 449–457.
[32] Ibanez, L., Schroeder, W., Ng, L., and Cates, J., 2005, *The ITK Software Guide*, 2nd ed., Kitware, New York.
[33] Collignon, A., Maes, F., Delaere, D., Vandermeulen, D., Suetens, P., and Marchal, G., 1995, "Automated Multi-Modality Image Registration Based on Information Theory," *Information Processing in Medical Imaging*, Y. Bizais, C. Barillot, and R. di Paola, eds., Kluwer Academic Publishers, Dordrecht, The Netherlands, pp. 263–274.
[34] Viola, P., and Wells, W. M., III, 1997, "Alignment by Maximization of Mutual Information," Int. J. Comput. Vis., **24**(2), pp. 137–154.
[35] Saha, P. K., and Chaudhuri, B. B., 1994, "Detection of 3D Simple Points for Topology Preserving," IEEE Trans. Pattern Anal. Mach. Intell., **16**(10), pp. 1028–1032.
[36] Saha, P. K., and Chaudhuri, B. B., 1996, "3D Digital Topology Under Binary Transformation With Applications," Comput. Vis. Image Understanding, **63**(3), pp. 418–429.
[37] Saha, P. K., Chaudhuri, B. B., and Majumder, D. D., 1997, "A New Shape Preserving Parallel Thinning Algorithm for 3D Digital Images," Pattern Recognit., **30**(12), pp. 1939–1955.
[38] Liu, X. S., Zhang, X. H., Sekhon, K. K., Adams, M. F., McMahon, D. J., Bilezikian, J. P., Shane, E., and Guo, X. E., 2010, "High-Resolution Peripheral Quantitative Computed Tomography Can Assess Microstructural and Mechanical Properties of Human Distal Tibial Bone," J. Bone Miner. Res., **25**(4), pp. 746–756.
[39] Guo, X. E., and Goldstein, S. A., 1997, "Is Trabecular Bone Tissue Different From Cortical Bone Tissue?," Forma, **12**, pp. 185–196.
[40] Hollister, S. J., Brennan, J. M., and Kikuchi, N., 1994, "A Homogenization Sampling Procedure for Calculating Trabecular Bone Effective Stiffness and Tissue Level Stress," J. Biomech., **27**(4), pp. 433–444.
[41] Feldkamp, L. A., Goldstein, S. A., Parfitt, A. M., Jesion, G., and Kleerekoper, M., 1989, "The Direct Examination of Three-Dimensional Bone Architecture In Vitro by Computed Tomography," J. Bone Miner. Res., **4**(1), pp. 3–11.
[42] Kabel, J., Odgaard, A., van Rietbergen, B., and Huiskes, R., 1999, "Connectivity and the Elastic Properties of Cancellous Bone," Bone, **24**(2), pp. 115–120.
[43] Kinney, J. H., and Ladd, A. J., 1998, "The Relationship Between Three-Dimensional Connectivity and the Elastic Properties of Trabecular Bone," J. Bone Min. Res., **13**(5), pp. 839–845.
[44] Odgaard, A., 1997, "Three-Dimensional Methods for Quantification of Cancellous Bone Architecture," Bone, **20**(4), pp. 315–328.
[45] Kostenuik, P. J., Capparelli, C., Morony, S., Adamu, S., Shimamoto, G., Shen, V., Lacey, D. L., and Dunstan, C. R., 2001, "OPG and PTH-(1–34) Have Additive Effects on Bone Density and Mechanical Strength in Osteopenic Ovariectomized Rats," Endocrinology, **142**(10), pp. 4295–4304.
[46] Pierroz, D. D., Bonnet, N., Baldock, P. A., Ominsky, M. S., Stolina, M., Kostenuik, P. J., and Ferrari, S. L., 2010, "Are Osteoclasts Needed for the Bone Anabolic Response to Parathyroid Hormone? A Study of Intermittent Parathyroid Hormone With Denosumab or Alendronate in Knock-in Mice Expressing Humanized RANKL," J. Biol. Chem., **285**(36), pp. 28164–28173.
[47] Samadfam, R., Xia, Q., and Goltzman, D., 2007, "Co-Treatment of PTH With Osteoprotegerin or Alendronate Increases Its Anabolic Effect on the Skeleton of Oophorectomized Mice," J. Bone Miner. Res., **22**(1), pp. 55–63.
[48] Campbell, G. M., Bernhardt, R., Scharnweber, D., and Boyd, S. K., 2011, "The bone Architecture is Enhanced With Combined PTH and Alendronate Treatment Compared to Monotherapy While Maintaining the State of Surface Mineralization in the OVX Rat," Bone, **49**(2), pp. 225–232.
[49] Tsai, J. N., Uihlein, A. V., Lee, H., Kumbhani, R., Siwila-Sackman, E., McKay, E. A., Burnett-Bowie, S. A., Neer, R. M., and Leder, B. Z., 2013, "Teriparatide and Denosumab, Alone or Combined, in Women With Postmenopausal Osteoporosis: The DATA Study Randomised Trial," Lancet, **382**(9886), pp. 50–56.
[50] Giuliani, N., Pedrazzoni, M., Negri, G., Passeri, G., Impicciatore, M., and Girasole, G., 1998, "Bisphosphonates Stimulate Formation of Osteoblast Precursors and Mineralized Nodules in Murine and Human Bone Marrow Cultures In Vitro and Promote Early Osteoblastogenesis in Young and Aged Mice In Vivo," Bone, **22**(5), pp. 455–461.
[51] Duque, G., and Rivas, D., 2007, "Alendronate has an Anabolic Effect on Bone Through the Differentiation of Mesenchymal Stem Cells," J. Bone Miner. Res., **22**(10), pp. 1603–1611.
[52] Fu, L., Tang, T., Miao, Y., Zhang, S., Qu, Z., and Dai, K., 2008, "Stimulation of Osteogenic Differentiation and Inhibition of Adipogenic Differentiation in Bone Marrow Stromal Cells by Alendronate Via ERK and JNK Activation," Bone, **43**(1), pp. 40–47.
[53] Tu, X., Rhee, Y., Condon, K. W., Bivi, N., Allen, M. R., Dwyer, D., Stolina, M., Turner, C. H., Robling, A. G., Plotkin, L. I., and Bellido, T., 2012, "Sost Down Regulation and Local Wnt Signaling are Required for the Osteogenic Response to Mechanical Loading," Bone, **50**(1), pp. 209–217.
[54] Bruel, A., Vegger, J. B., Raffalt, A. C., Andersen, J. E., and Thomsen, J. S., 2013, "PTH (1–34), But Not Strontium Ranelate Counteract Loss of Trabecular Thickness and Bone Strength in Disuse Osteopenic Rats," Bone, **53**(1), pp. 51–58.
[55] Turner, C. H., Warden, S. J., Bellido, T., Plotkin, L. I., Kumar, N., Jasiuk, I., Danzig, J., and Robling, A. G., 2009, "Mechanobiology of the Skeleton," Sci. Signaling, **2**(68), p. pt3.